Electronic Supplementary Material (ESI) for Materials Horizons.
This journal is © The Royal Society of Chemistry 2023

Supporting Information

Rapid Carbothermal Shocking Fabrication of Iron-Incorporated Molybdenum Oxide with Heterogeneous Spin States for Enhanced Overall Water/Seawater Splitting

Jianpeng Sun[1], Shiyu Qin[1], Zhan Zhao[1], Zisheng Zhang[2] and Xiangchao Meng[1]*

[1]Key Laboratory of Marine Chemistry Theory and Technology, Ministry of Education, College of Chemistry and Chemical Engineering, Ocean University of China, Qingdao 266100, China

[2]Department of Chemical and Biological Engineering, Faculty of Engineering, University of Ottawa, Ottawa, Ontario, K1N6N5, Canada.

**Corresponding author, E-mail: mengxiangchao@ouc.edu.cn*

S1. Experimental section

Chemicals and reagents: Ferric nitrate nonahydrate ($Fe(NO_3)_3·9H_2O$) and ammonium molybdate tetrahydrate ($(NH_4)_6Mo_7O_{24}·4H_2O$) were purchased from Aladdin Reagent Inc (China) and were used in this work without further treatment. Ni foams were purchased from Kunshan Guangjiayuan New Materials Co. Ltd. Hydrochloric acid was obtained from Sinopharm Chemical Reagent Co. Ltd.

Preparation of FeMoO/NF: First, hydrochloric acid (2 M) were used to clean and remove impurities on the commercial nickel foam (NF). And then, $Fe(NO_3)_3·9H_2O$ (175 mg) and $(NH_4)_6Mo_7O_{24}·4H_2O$ (185 mg) were separately dispersed in 15 mL of deionized (DI) water. Then, the mixture was transferred into an autoclave, and a piece of NF (1 cm × 2 cm) was vertically immersed into the solution, which was kept at 150°C for 6 h. FeMoO/NF was dried at 70°C under vacuum, and then collected. And MoO_3/NF was designed using a method similar to the preparation method of FeMoO/NF except no $Fe(NO_3)_3·9H_2O$ was added. Moreover, CoMoO/NF and NiMoO/NF were designed using a method similar to the preparation method of FeMoO/NF except that $Co(NO_3)_2·6H_2O$ and $Ni(NO_3)_2·6H_2O$ was added without $Fe(NO_3)_3·9H_2O$.

Preparation of Fe-MoO

the preparation method of Fe-MoO_2/NF.

Preparation of MoO_2/NF: MoO_2/NF were prepared using a method similar to the preparation method of Fe-MoO_2/NF. A piece of MoO_3/NF (1 cm × 0.5 cm) was placed on a graphite heating plate and heated at 820 °C for 127 seconds under Ar-H_2 flow. And then, MoO_2/NF was collected.

Electrochemical measurements: Electrocatalytic activity of NF, MoO_2/NF, FeMoO/NF, MoO_3/NF was calculated on a CHI660E electrochemical workstation with a typical three-electrode system. Graphite rod and a Hg/HgO electrode were used as the counter electrode and the reference electrode, respectively. The applied potentials were converted by the equation ($E_{RHE} = E_{Hg/HgO} + 0.0592\text{pH} + 0.098$ V) and the polarization curves were recorded with *iR* compensation. Alkaline seawater (pH = 13.8) was prepared by dissolving 28.06 g of potassium hydroxide in natural seawater (pH = 8.6) in a 500-mL volumetric bottle. The supernate was separated out for further use in the electrochemical tests. Natural seawater was collected from Yellow Sea (35°56′N, 120°56′E). The chlorine content was about 0.55 M. The alkaline seawater electrolyte was saturated with N_2. Linear sweep voltammetry (LSV) was performed at a scan rate of 5 mV s^{-1}). And the polarization curves were recorded with 100% iR-compensation, which were automatically compensated by the machine. The double layer capacitance (C_{dl}) values were determined from the CV curves at various scan rates to investigate the electrochemically active surface areas (ECSA). C_{dl} was calculated from CV according to the following equation:

$$Cdl = (j_a - j_c)/(2 \cdot v) = (j_a + |j_c|)/(2 \cdot v) = \Delta j/(2 \cdot v)$$

in which j_a and j_c is the anodic and cathodic voltammetric current density, respectively, recorded at the middle of the selected potential range, and v is the scan rate.

The electrochemical impedance spectroscopy (EIS) measurements were used with frequencies ranging from 10^5 Hz to 10^{-2} Hz at -17 mV (*vs.* RHE) in alkaline seawater. The stability tests were conducted under a current density of 100 mA·cm^{-2}. The faradaic efficiency (FE) was tested by drainage method. The polarization characteristics of alkaline exchange membrane (AEM) electrolyzers without iR compensation were measured on a CHI660E electrochemical workstation at a scan rate of 10 mV s^{-1}. The anion-exchange membrane (FAA-3–50) was purchased from Suzhou Sinero Technology Co., Ltd. The dimensions of the Fe-MoO_2/NF electrodes was 2*2 cm^2.

5 mg Pt/C / RuO_2 was dispersed into 0.5-mL mixed solution (Nafion: ethanol: water = 1:9:10) and formed a homogeneous ink. 0.4-mL ink was dropped onto the NF electrode (1·cm^{-2}). The mass loading of Pt/C / RuO_2 was about 4 mg cm^{-2}.

The solar-driven electrolysis system was carried out by the KEITHLEY 2400 and CHI660, solar simulator was used via a 300-W xenon lamp with AM 1.5G optical filter (100 mW cm^{-2}). $STH(\%) = I(mA\ cm^{-2}) \times 1.23(V) \times 100/P_{sun}$ was used as the equation to study the solar-hydrogen efficiency of the solar-driven electrolytic system, where I was the current density of the solar-driven electrolysis system and P_{sun} was incident simulated solar energy.

Calculation of energy consumption per unit of hydrogen production:

$W_{H2} = (I \bullet \int U \bullet dt)/(Q_{H2} \bullet 10^3)$

Where W_{H_2} (kW·h/m^3) was the hydrogen production electricity consumption, I (A) and U (V) were the current and voltage in the electrolyzer, the t (h) was time and the Q_{H_2} (m^3) is the volume of the produced hydrogen. Among them, the amount of the hydrogen production was obtained using the drainage method. And the current and the hydrogen production were measured in 10 min.

Colorimetric detection experiment: the concentrations of free chlorine (i.e. Cl_2, HClO and ClO^-) were determined by colorimetric method. The solutions (20 mL of electrolyte) were neutralized with HCl solution to a pH between 6 and 7, and mixed with 45 mL phosphate buffer (pH = 6.5) and 5 mL N, N -diethyl-1,4-phenylenediamine sulfate (DPD; 1.1 g/L) solution. Under these conditions, free chlorine reacts directly with DPD to form a colored dye (Worcester dye). The absorbance was determined by UV-Vis absorption spectroscopy (Persee TU-1901). Alkaline seawater electrolytes with different NaClO contents and post-tested electrolytes after 24 h electrolysis of 100 mA cm^{-2} were analyzed.

Perovskite solar cells (PSC) fabrication:

Polymer solar cells were manufactured in a glove box with temperature of 20 ° C, oxygen of 0.1 ppm and water of 0.1 ppm. First, D18, Y6 and BTP-eC9 were dissolved in chloroform, and 0.5 vol.% of 1,8-diiodooctane (DIO) was added. The device was manufactured on the indium tin oxide (ITO) glass substrate with conventional structure of ITO/PEDOT: PSS/active layer/PDINO/Al. Among them, ITO substrates were ultrasonically treated in detergent, deionized water, acetone and isopropanol for 25 minutes, and then in ultraviolet ozone chamber for 5 minutes, and then at 150 ° C for 15 minutes. ITO was then placed in the glove box. The active layer was rotated onto the PEDOT: PSS layer at 3000 RPM for 35 seconds. The PDINO layer (1 mg mL^{-1} in methanol) was applied to the active layer at 3000 rpm for 25 seconds. Finally, Al with the thickness of 80 nm was deposited through shadow masks (0.07 cm^2) by thermal evaporation under 4×10^{-4} Pa to obtain PSC.

DFT computations:

We performed theoretical calculations by using the Vienna ab initio software package (VASP). The computational procedure employed the gradient approximation (GGA) with the Perdew-Burke-Ernzerhof (PBE) parameterization to represent the exchange-correlation energies. The cutoff energy of employed planewave basis set was 500 eV and the structural relaxation was tested with an energy convergence criterion of 10^{-5} eV. The vacuum layer was 15 Å. Fe-MoO_2 and MoO_2 were modeled using a 3 × 3 × 1 k-point mesh in the Brillouin zone. Among them, (002) facet of MoO_2 model was used to study the electronic structure. And Fe-MoO_2 model was designed to replace a single Mo atom by a Fe atom. The adsorption free energies were obtained by including the zero point energy (ZPE) and the entropy (S) corrections in equation:

$$\Delta G = \Delta E + \Delta ZPE - T\Delta S$$

Where ΔE was reaction heats of a certain reaction step. The ΔZPE could be obtained from the calculation of vibrational frequencies for the adsorbed species, and the T was temperature.

Characterization: Scanning electron microscope (SEM) and high-resolution transmission electron microscopy (HRTEM) were characterized by Zeiss Gemini 300 and JEOL JEM 2100, respectively. X-ray diffraction (XRD) was collected on the Rigaku Miniflex 600. The energy dispersive X-ray (EDX) element mapping images were tested on the SEM equipped. The X-ray photoelectron spectroscopy (XPS) spectra were collected on Thermo Scientific K-Alpha. The Brunauer-Emmett-Teller (BET) surface area and Barrett−Joyner−Halenda model were collected on the Micromeritics ASAP 2460. Xenon Lamp Source (Microsolar300) was purchased from Beijing Perfectlight. A Dataphysics OCA 20 contact angle system was used to test the hydrophilicity of the electrodes. X-ray absorption near-edge structure (XANES) and extended X-ray absorption fine structure (EXAFS) were performed with Si (111) crystal monochromators at the BL14W Beam line at the Shanghai Synchrotron Radiation

Facility (SSRF) (Shanghai, China). The spectra were processed and analyzed by the software codes Athena.

S2 Figure

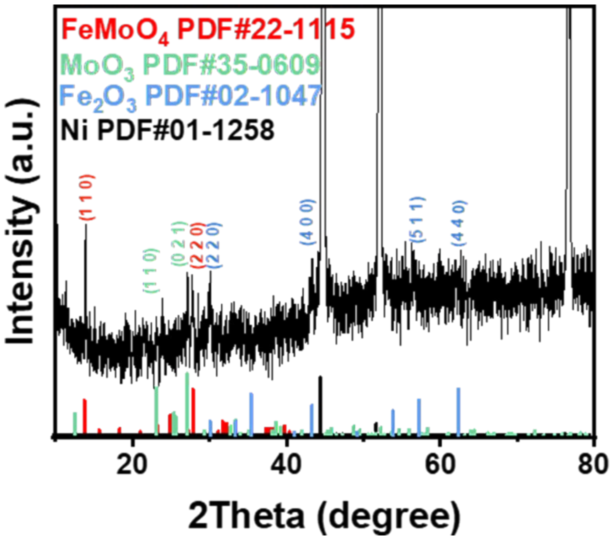

Figure S1. The XRD of FeMoO/NF.

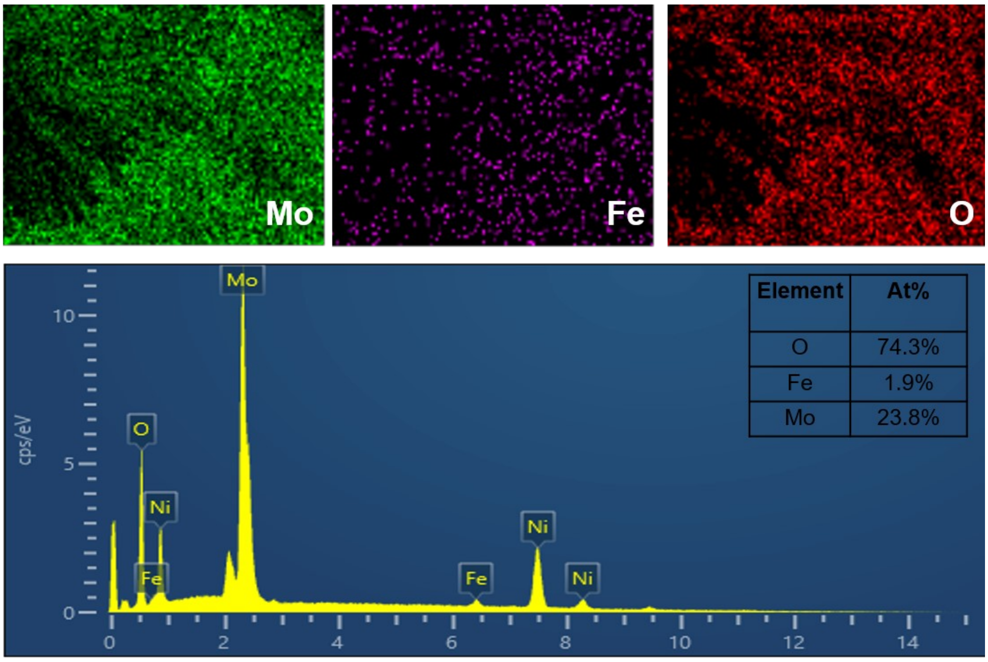

Element	At%
O	74.3%
Fe	1.9%
Mo	23.8%

Figure S2. EDS mapping of FeMoO/NF

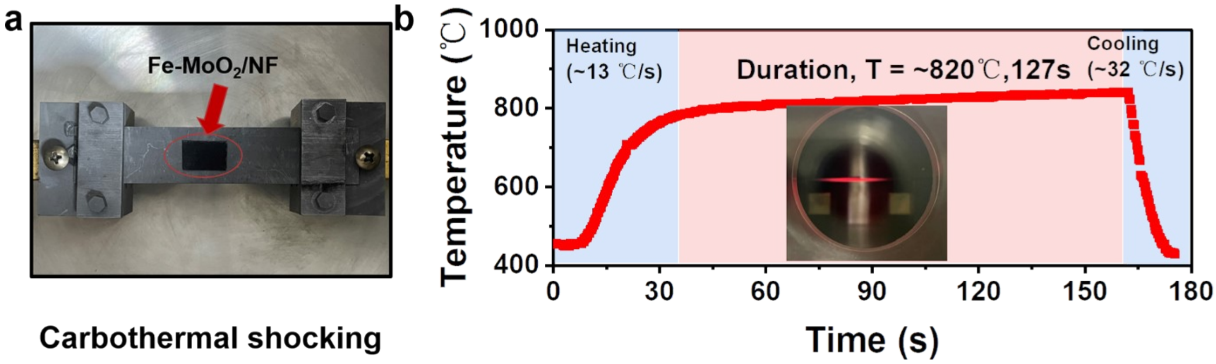

Figure S3. (a) Carbothermal Shocking process photograph of Fe-MoO$_2$/NF. (b) Real time reaction temperature of Joule heating process.

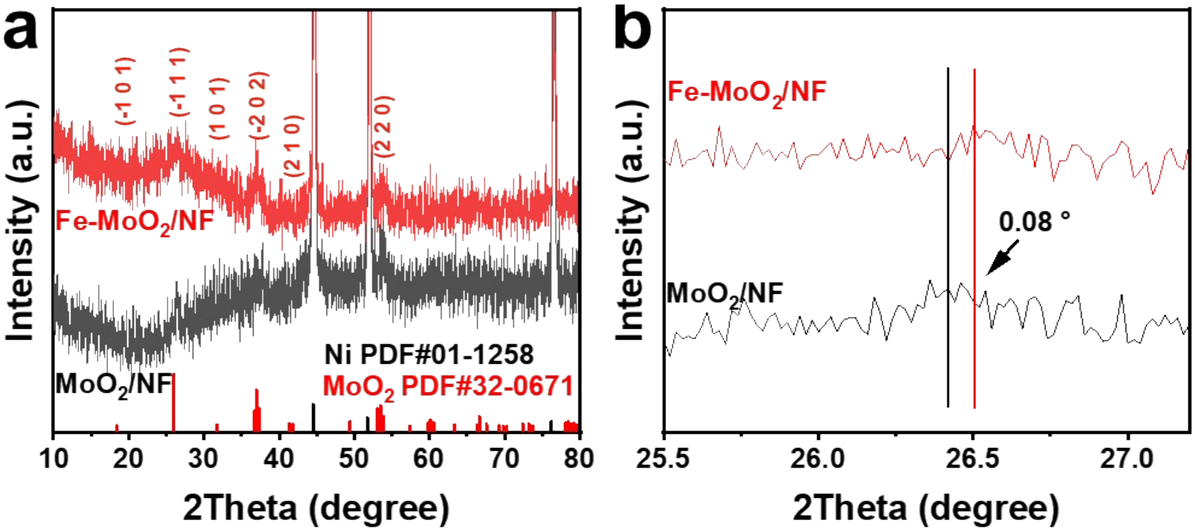

Figure S4. The XRD of Fe-MoO$_2$/NF and MoO$_2$/NF.

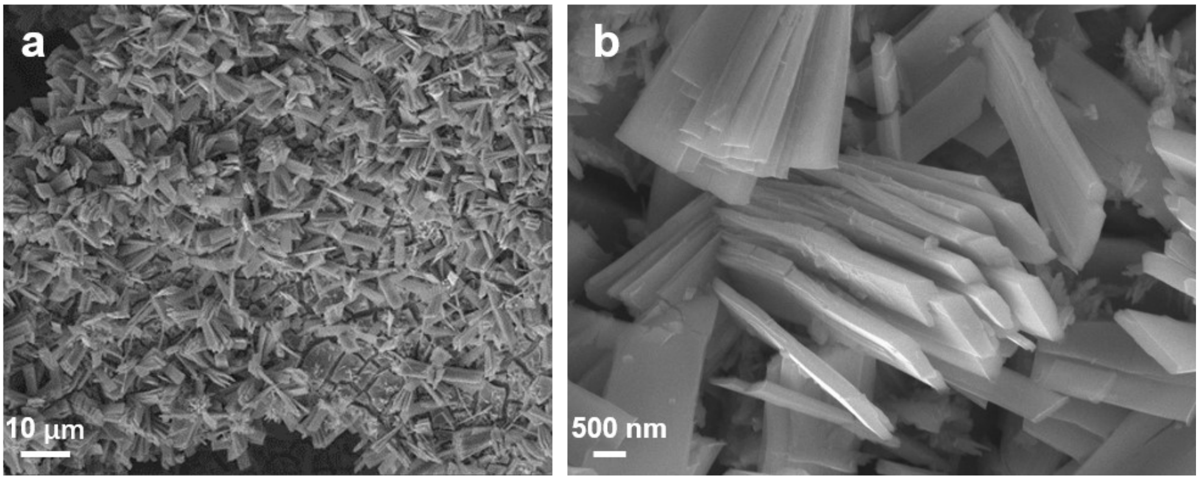

Figure S5. (a, b) SEM image of MoO_2/NF.

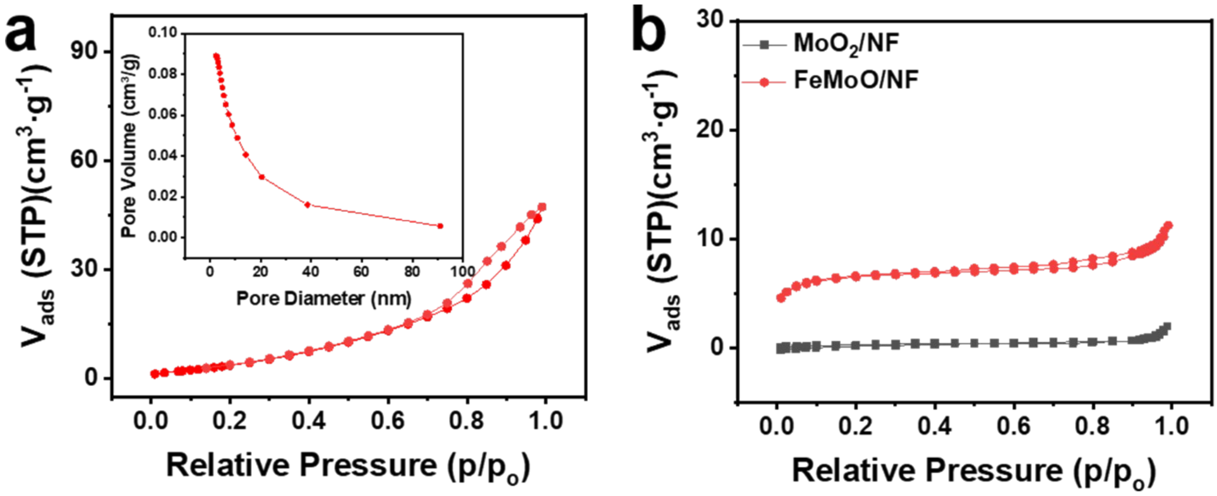

Figure S6. N_2 adsorption–desorption isotherms of (a) Fe-MoO_2/NF (the inset shows the pore size distribution curve), (b) MoO_2/NF and FeMoO/NF.

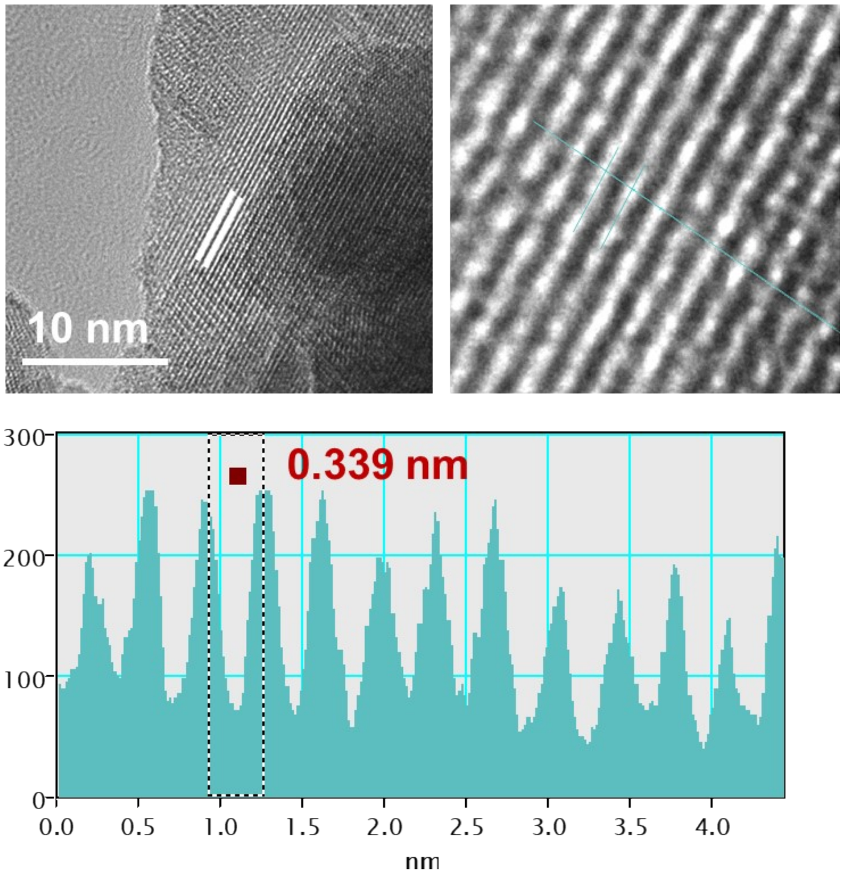

Figure S7. HRTEM analysis of MoO_2/NF.

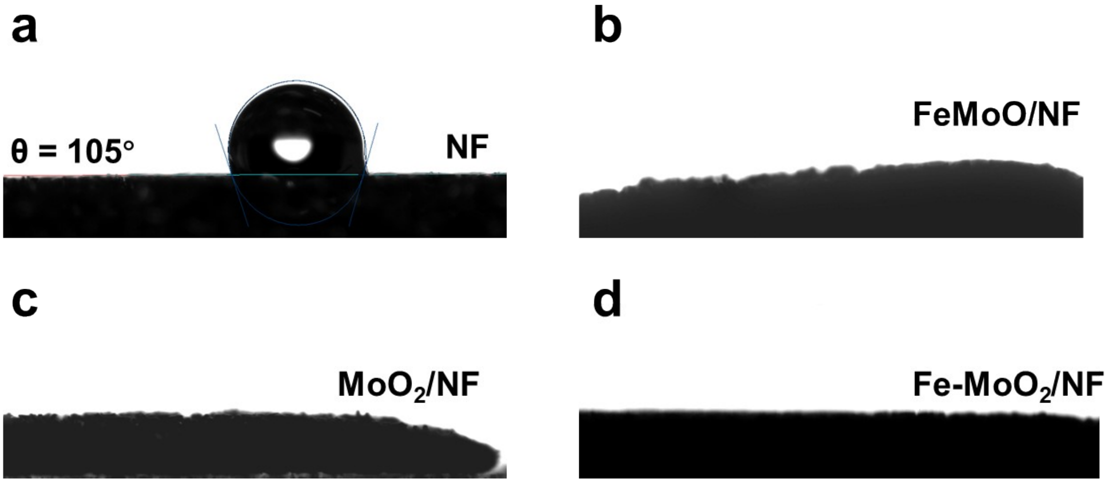

Figure S8. The droplet contacts angle images of the (a) bare NF, (b) FeMoO/NF, (c) MoO_2/NF and (d) Fe-MoO_2/NF.

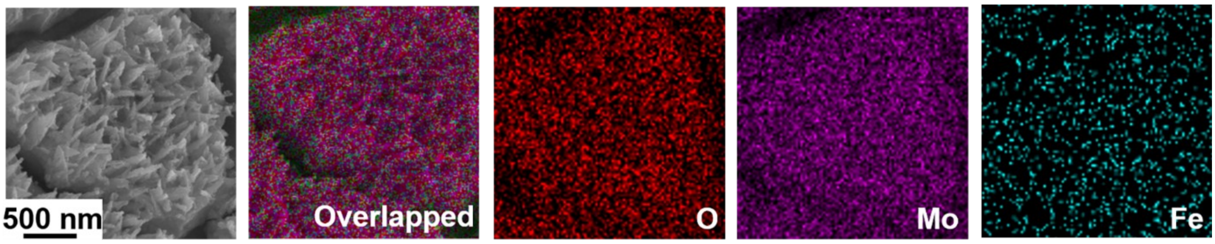

Figure S9. EDS mapping of Fe-MoO_2/NF.

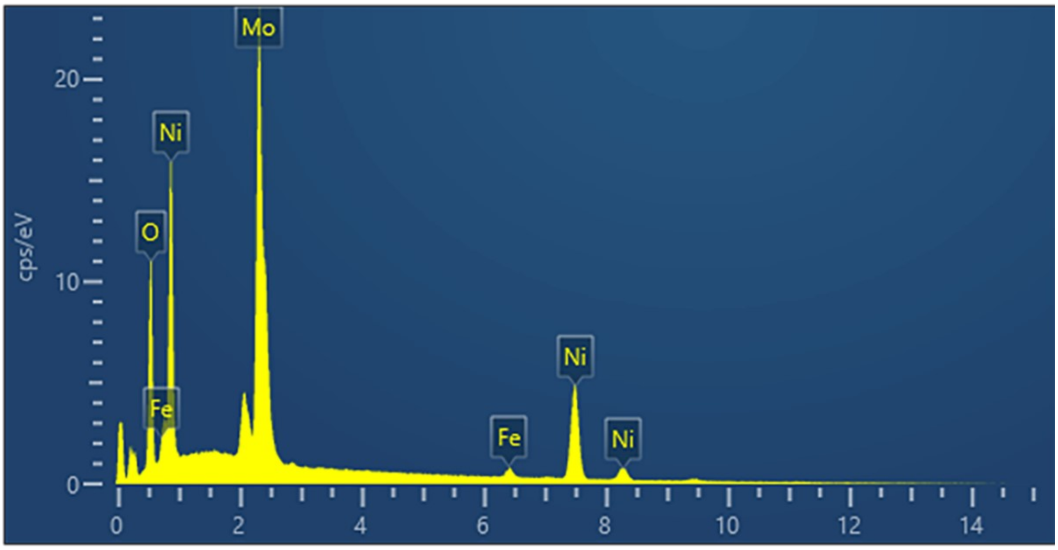

Figure S10. EDS spectrum of Fe-MoO_2/NF.

Compared with FeMoO/NF, the Mo:Fe ratio in Fe-MoO_2/NF (Fe:Mo:O=2.1%:27.8%:70.1%) changes from 12.53 to 13.24, which is very close. Among them, it does not conform to the 1/2 relationship corresponding to the Fe/Mo molar feed ratio in FeMoO/NF, which is mainly due to the fact that the metal ions in the solution are not completely grown on the surface of the nickel foam in the synthesis, and part of them forms Fe-rich powder precipitation.

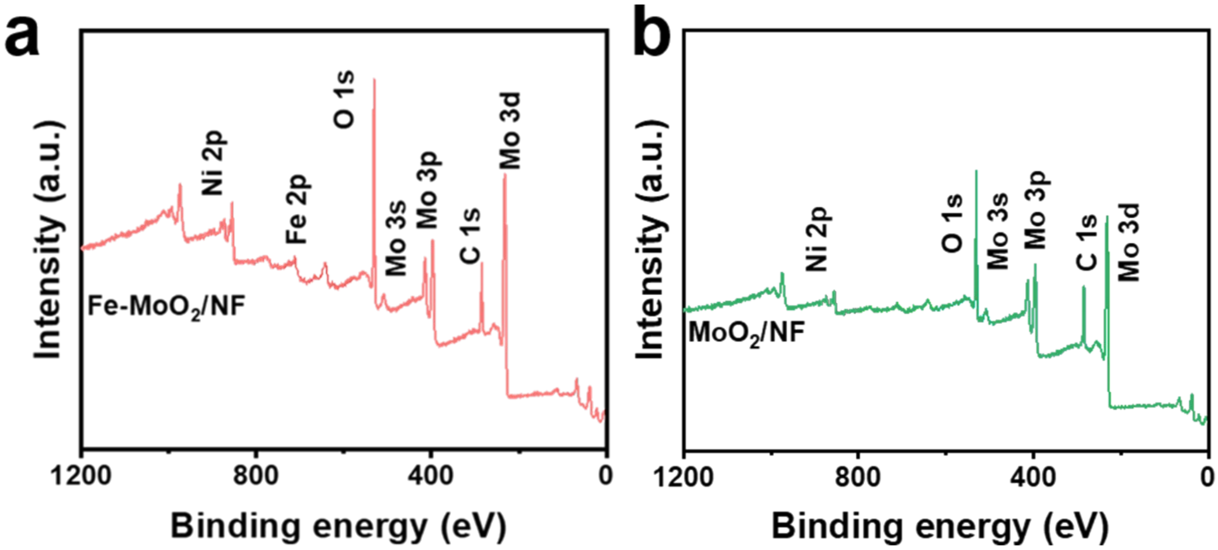

Figure S11. XPS survey spectrum of (a) Fe-MoO_2/NF and (b) MoO_2/NF.

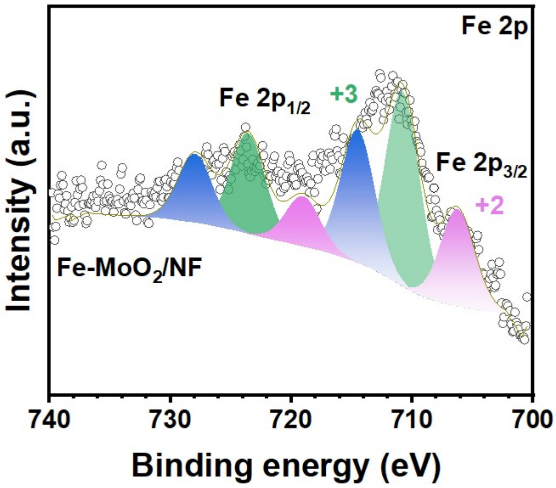

Figure S12. Fe 2p of Fe-MoO$_2$/NF.

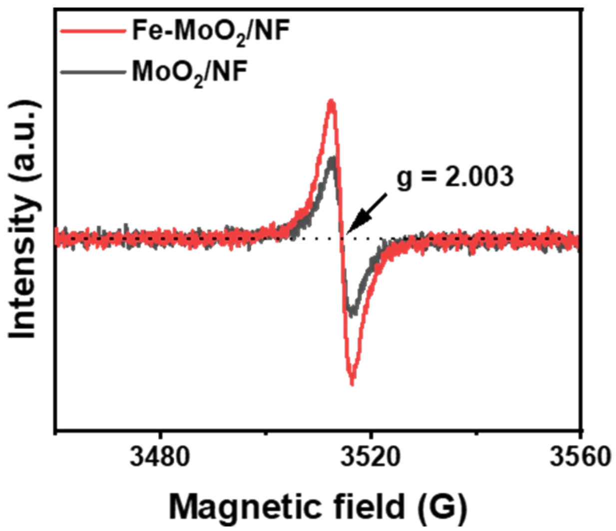

Figure S13. EPR spectrum of Fe-MoO$_2$/NF and MoO$_2$/NF.

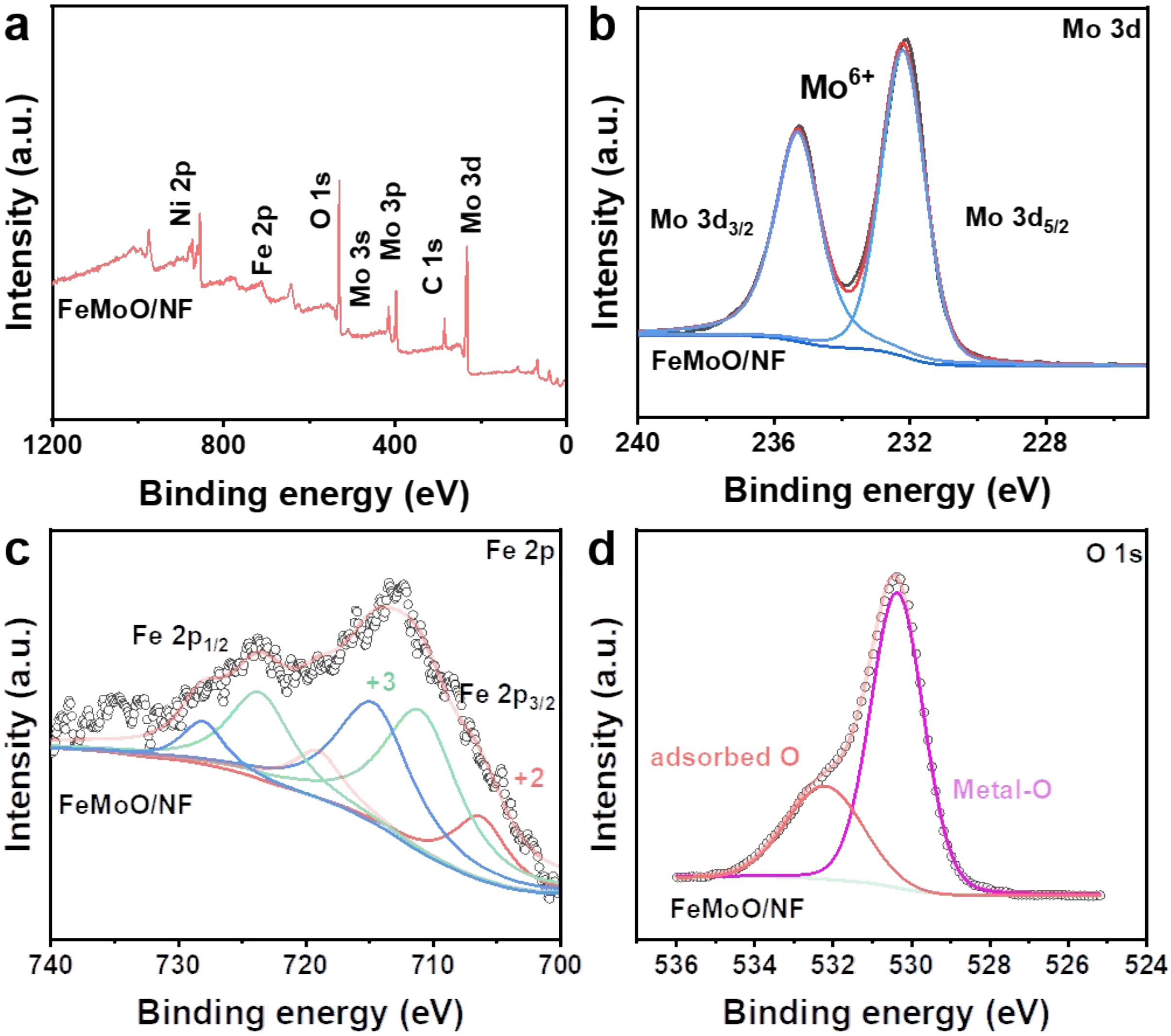

Figure S14. (a) XPS survey spectrum and high-resolution spectra of: (b) Mo 3d, (c) Fe 2p, and (d) O 1s for FeMoO/NF.

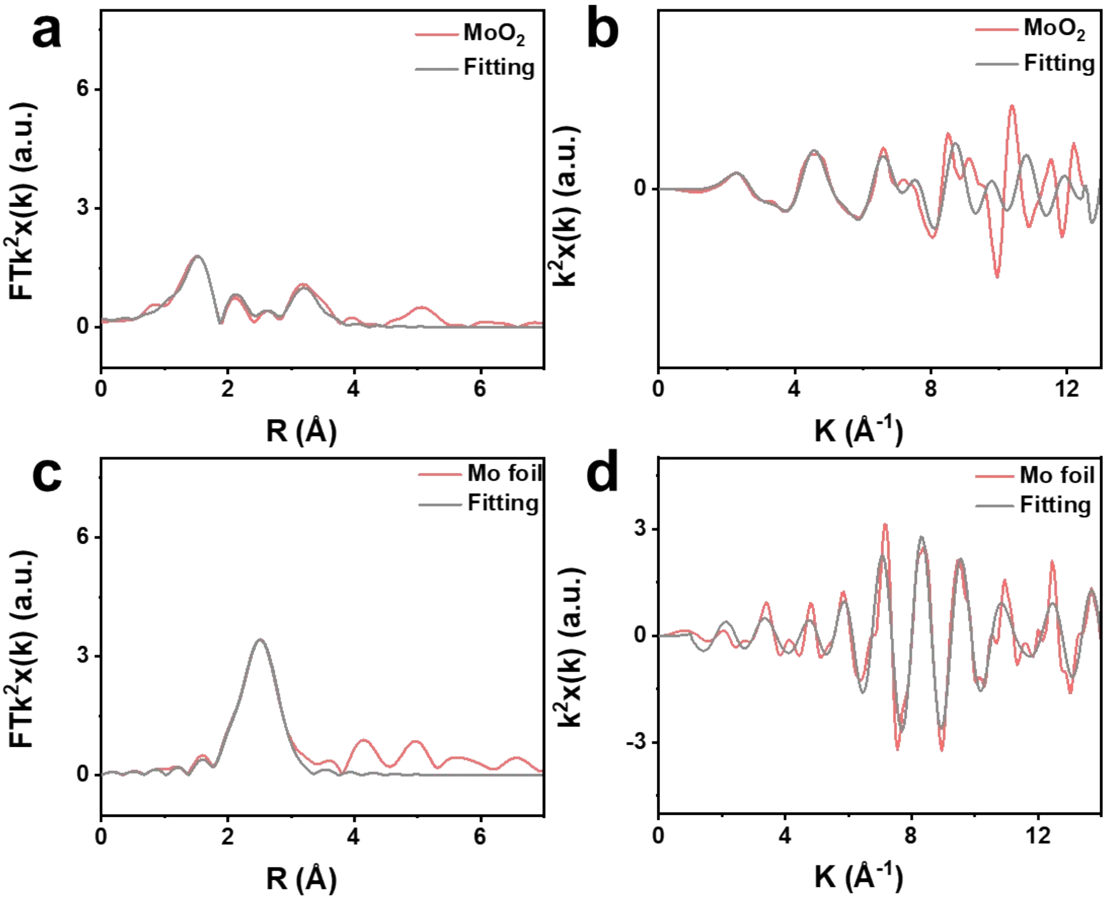

Figure S15. (a) K-space and (b) R-space of MoO$_2$ in the Mo K-edge. (c) K-space and (d) R-space of Mo foil in the Mo K-edge.

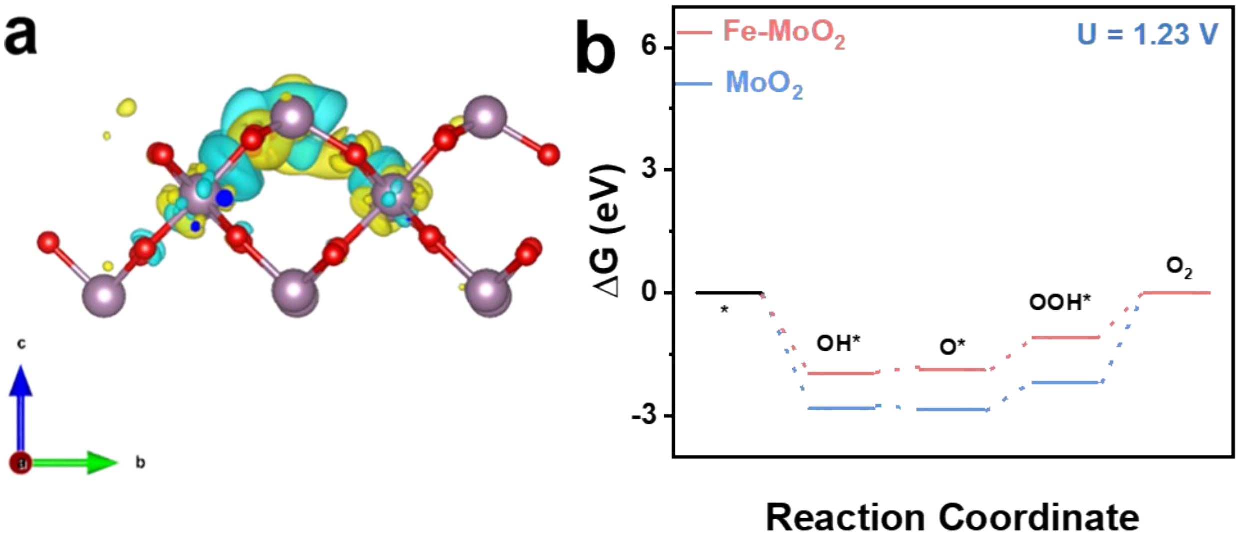

Figure S16. (a) Atomic models with charge density difference plot of Fe-MoO$_2$. The yellow and cyan contours represent charge accumulation and depletion, respectively. (b) Free energy diagrams of OER (U = 1.23 V).

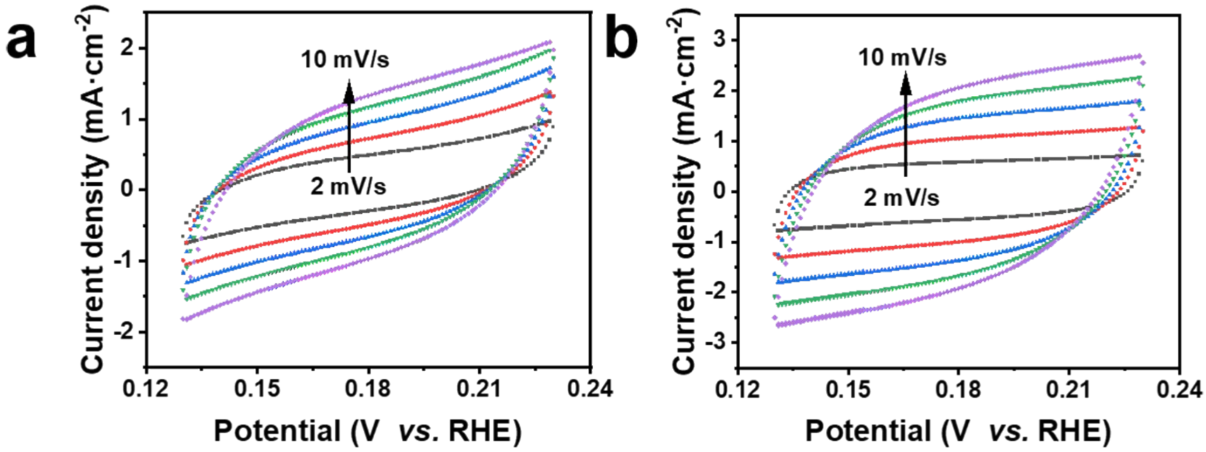

Figure S17. Alkaline seawater: CV curves of (a) MoO_2/NF, (b) Fe-MoO_2/NF.

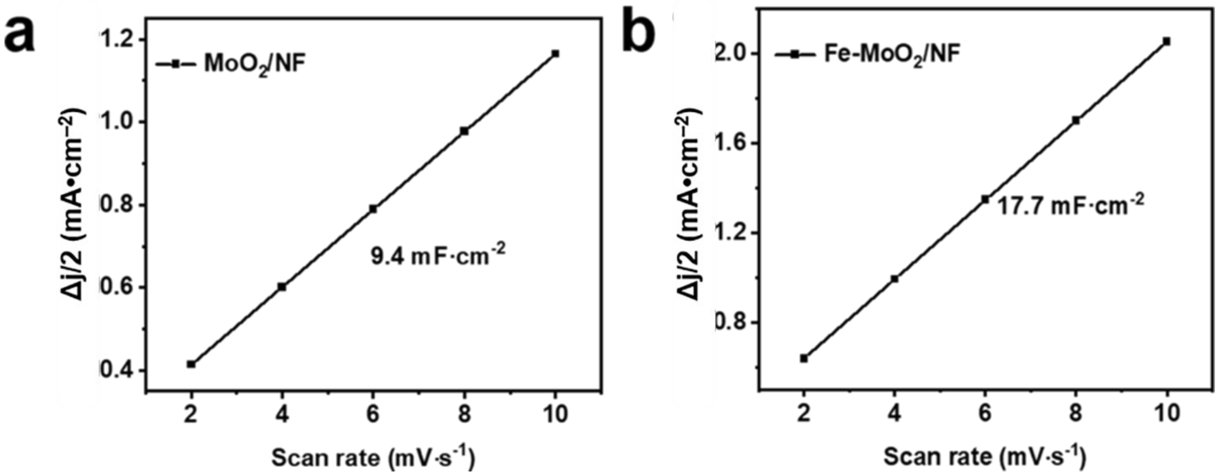

Figure S18. Alkaline seawater: electrochemical double layer capacitance (C_{dl}) of (a) MoO_2/NF, (b) Fe-MoO_2/NF.

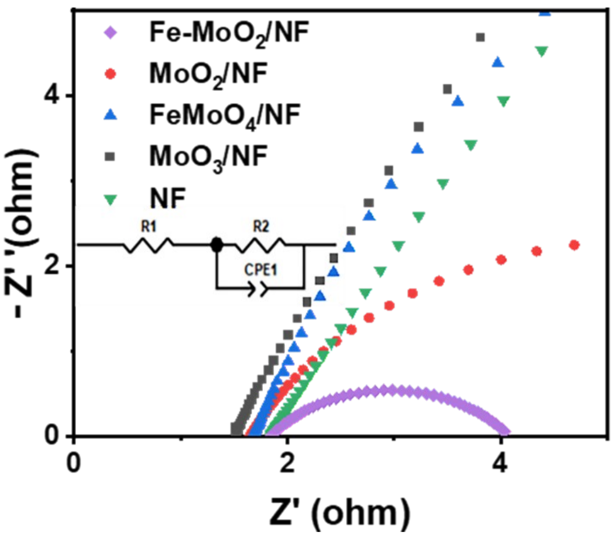

Figure S19. Alkaline seawater: EIS of Fe-MoO_2/NF, MoO_2/NF, FeMoO/NF and MoO_3/NF.

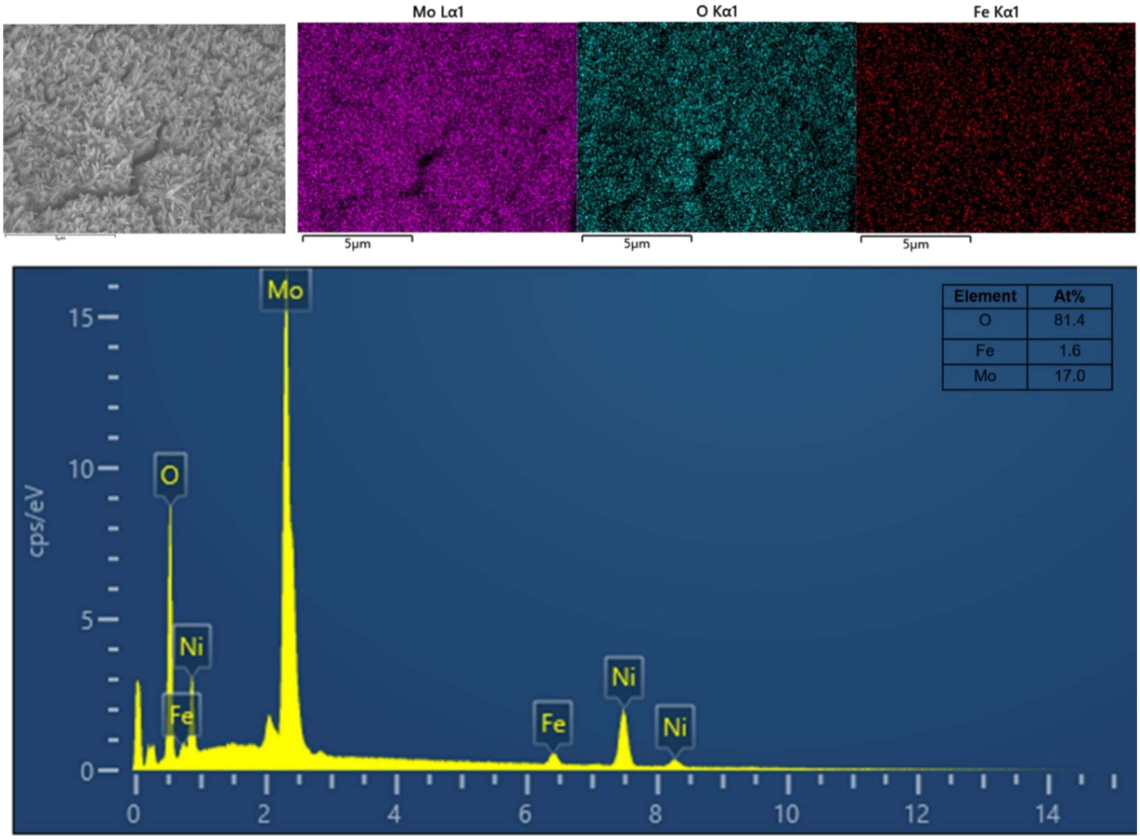

Figure S20. EDS mapping of Fe-MoO_2/NF after HER process.

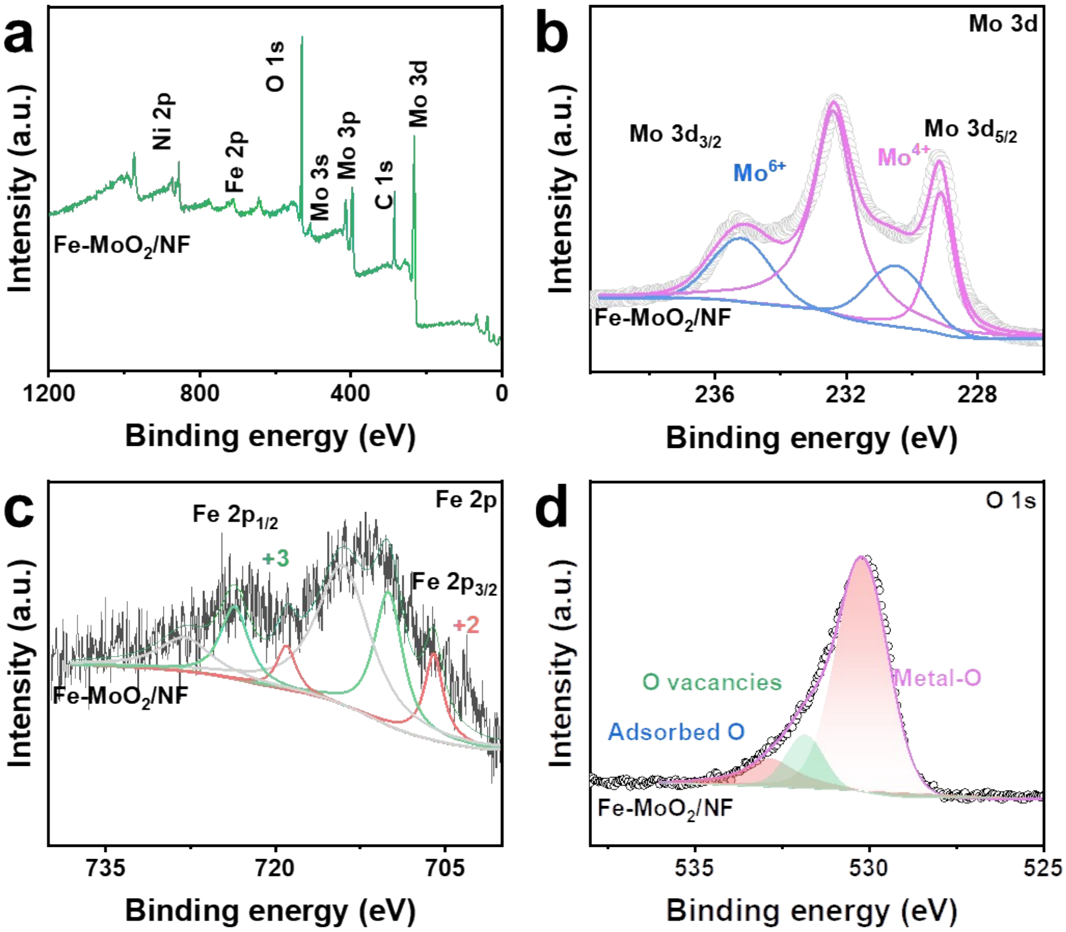

Figure S21. (a) XPS survey spectrum and high-resolution spectra of: (b) Mo 3d, (c) Fe 2p, and (d) O 1s for Fe- MoO_2/NF after HER process.

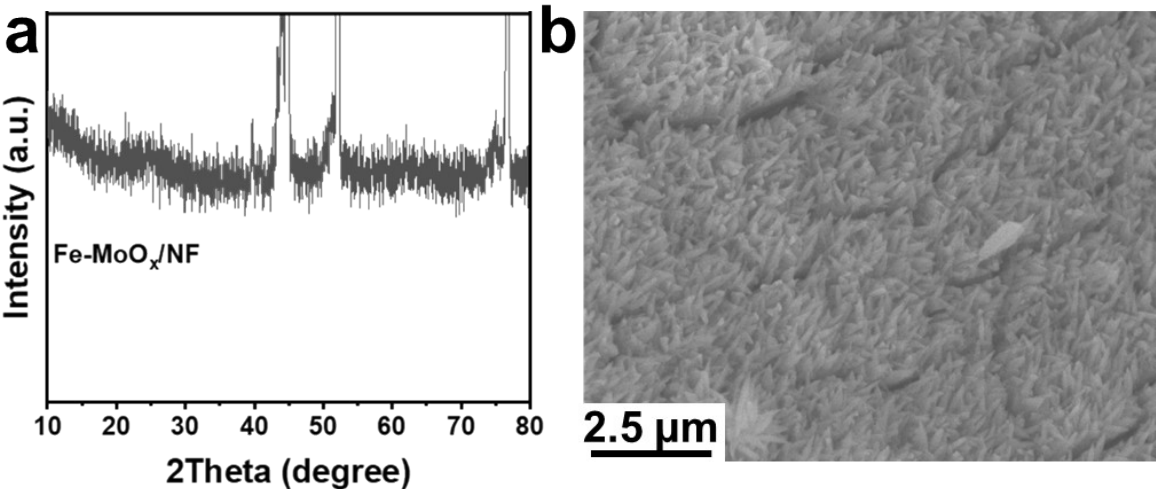

Figure S22. (a) XRD and (b) SEM of Fe-MoO$_x$/NF.

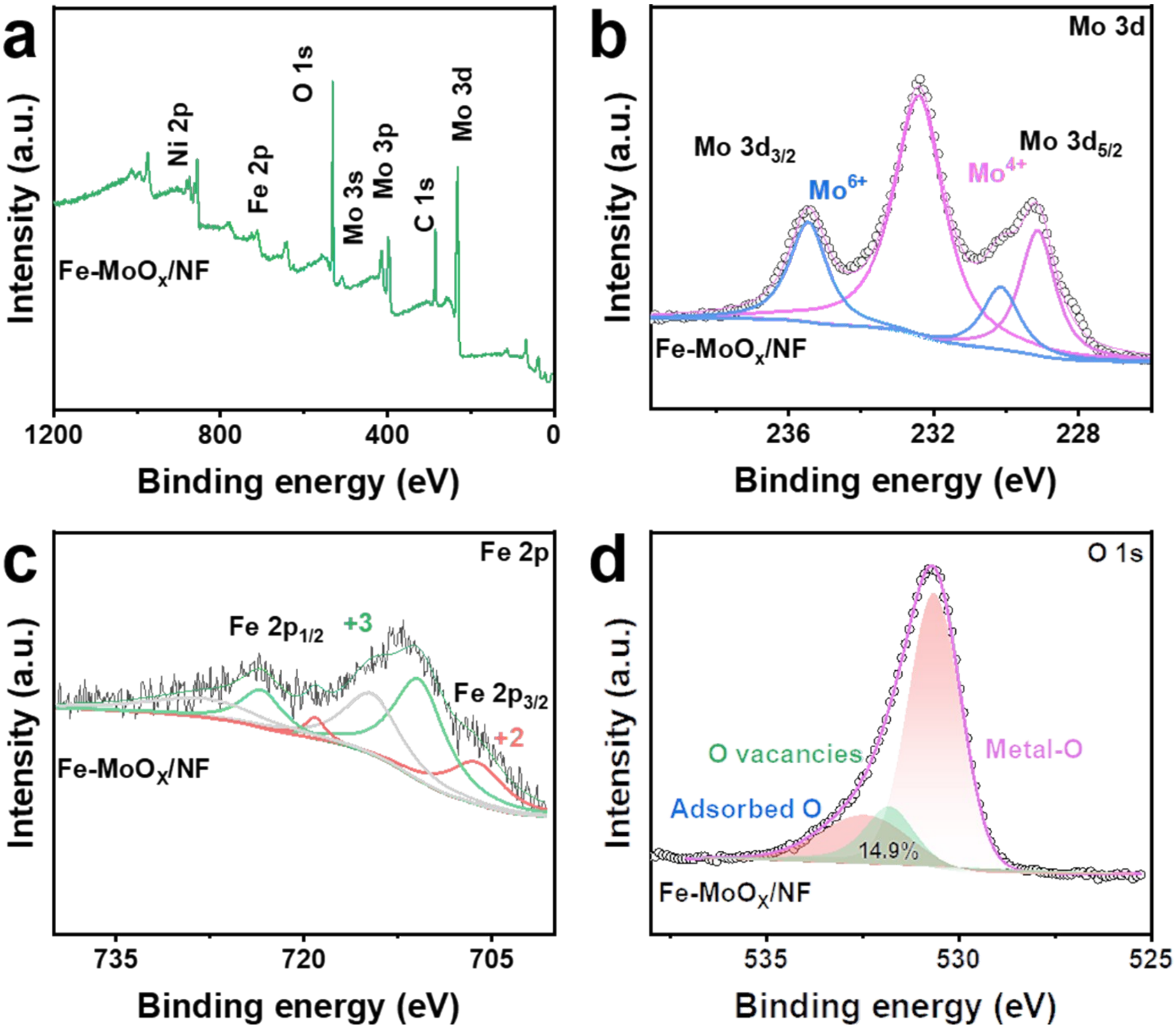

Figure S23 (a) XPS survey spectrum, XPS spectra of (b) Mo 3d, (c) Fe 2p, (d) O 1s in Fe-MoO$_X$/NF.

Mo^{4+} (229.1/232.4 eV) and Mo^{6+} (230.1/235.4 eV) were shown in the Mo 3d$_{5/2}$/3d$_{3/2}$ XPS spectrum of Fe-MoO$_x$/NF. The Fe 2p$_{3/2}$/2p$_{1/2}$ XPS spectrum of Fe-MoO$_x$/NF showed three pairs of peaks derived from Fe^{2+} (706.2/719.1 eV) and Fe^{3+} (710.8/723.4 eV) and satellite peaks. The O 1s spectrum could be associated with metal-oxygen bond (530.6 eV), O vacancies (531.8 eV) and adsorption of oxygen (532.5 eV).

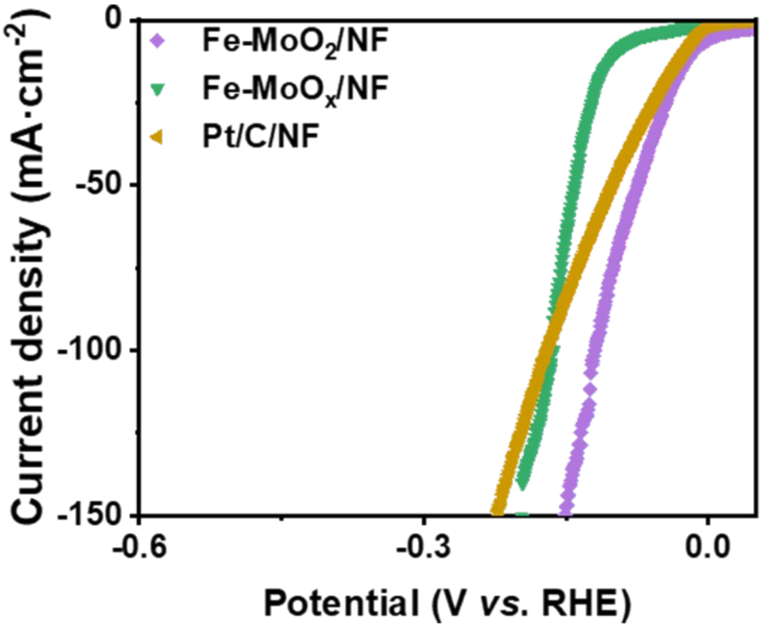

Figure S24 (a) LSV performance of Fe-MoO$_X$/NF and Fe-MoO$_X$/NF in alkaline seawater.

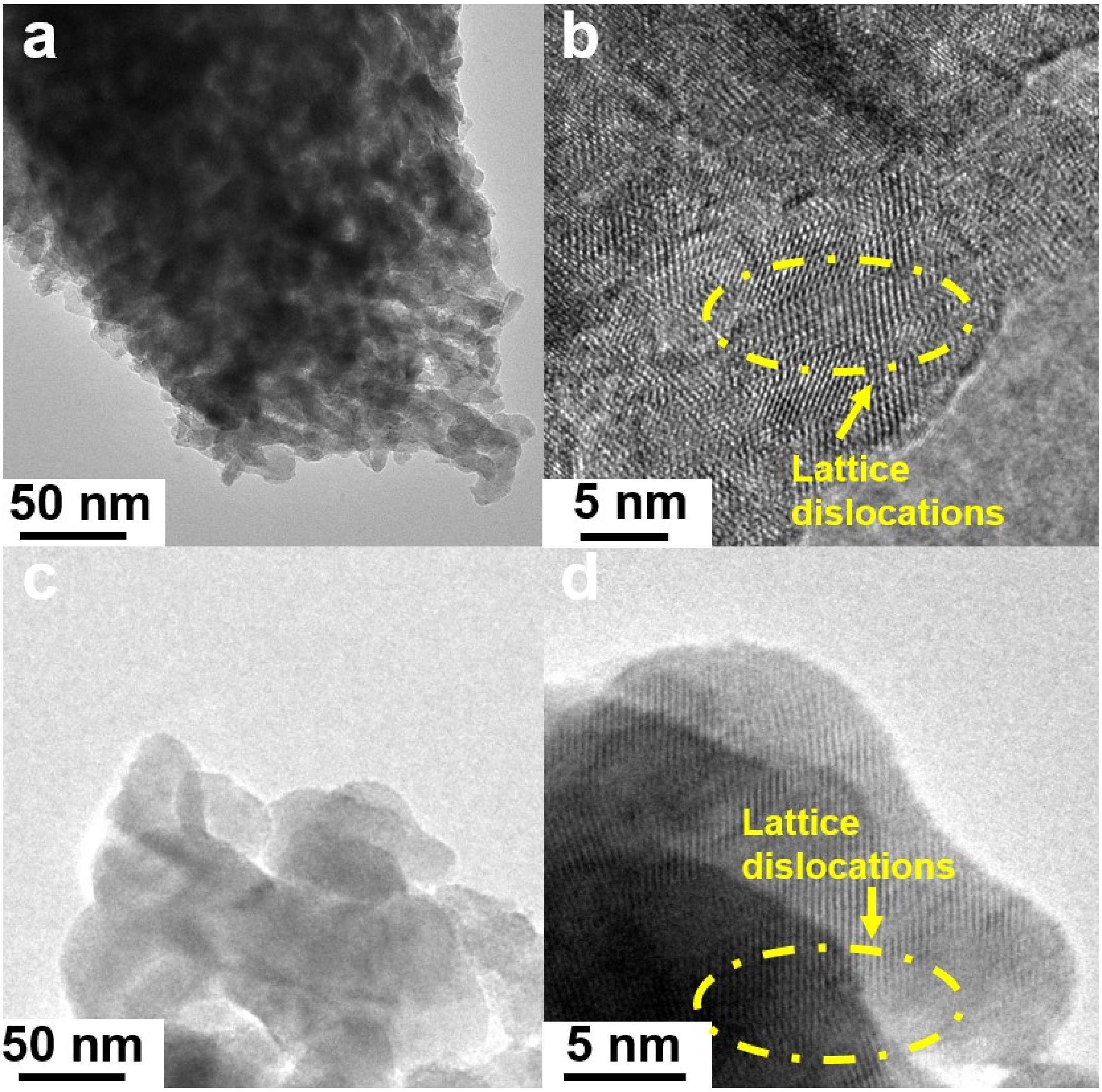

Figure S25 (a) TEM image and (b) HRTEM images of Co-MoO_2/NF. (c) TEM image and (d) HRTEM images of Ni-MoO_2/NF

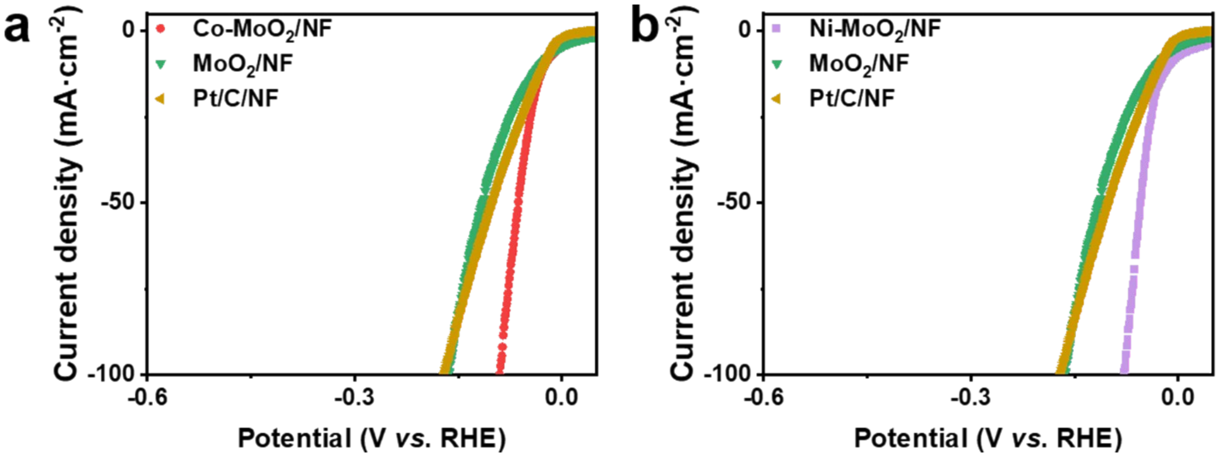

Figure S26 (a) LSV performance of Co--MoO$_2$/NF and Ni-MoO$_2$/NF in alkaline seawater.

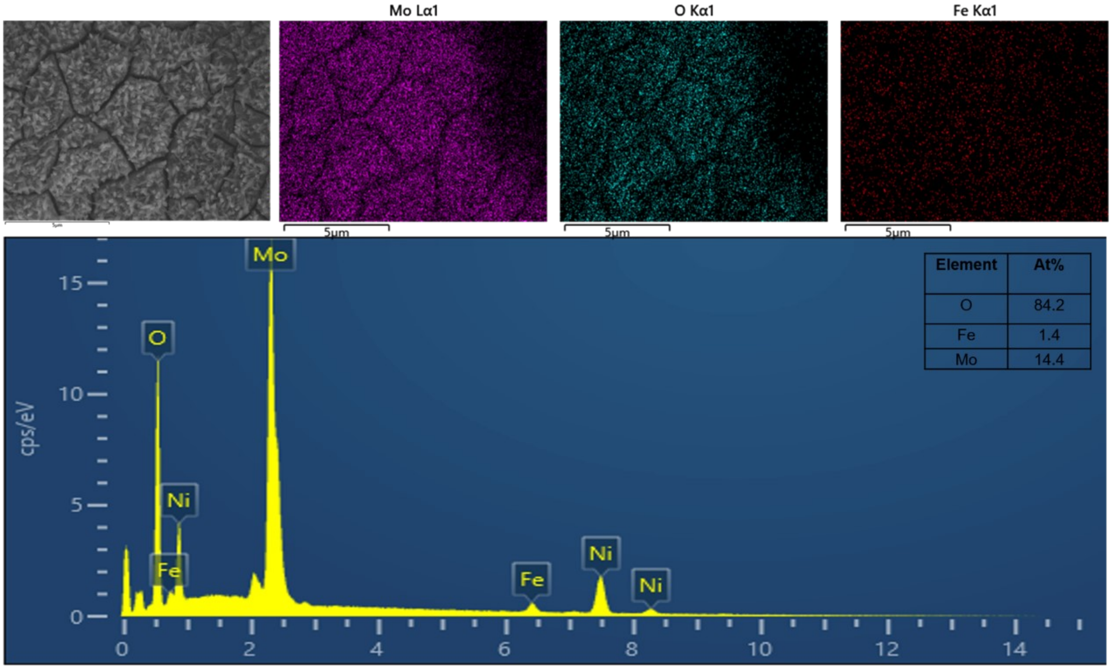

Figure S27. EDS mapping of Fe-MoO_2/NF after OER process.

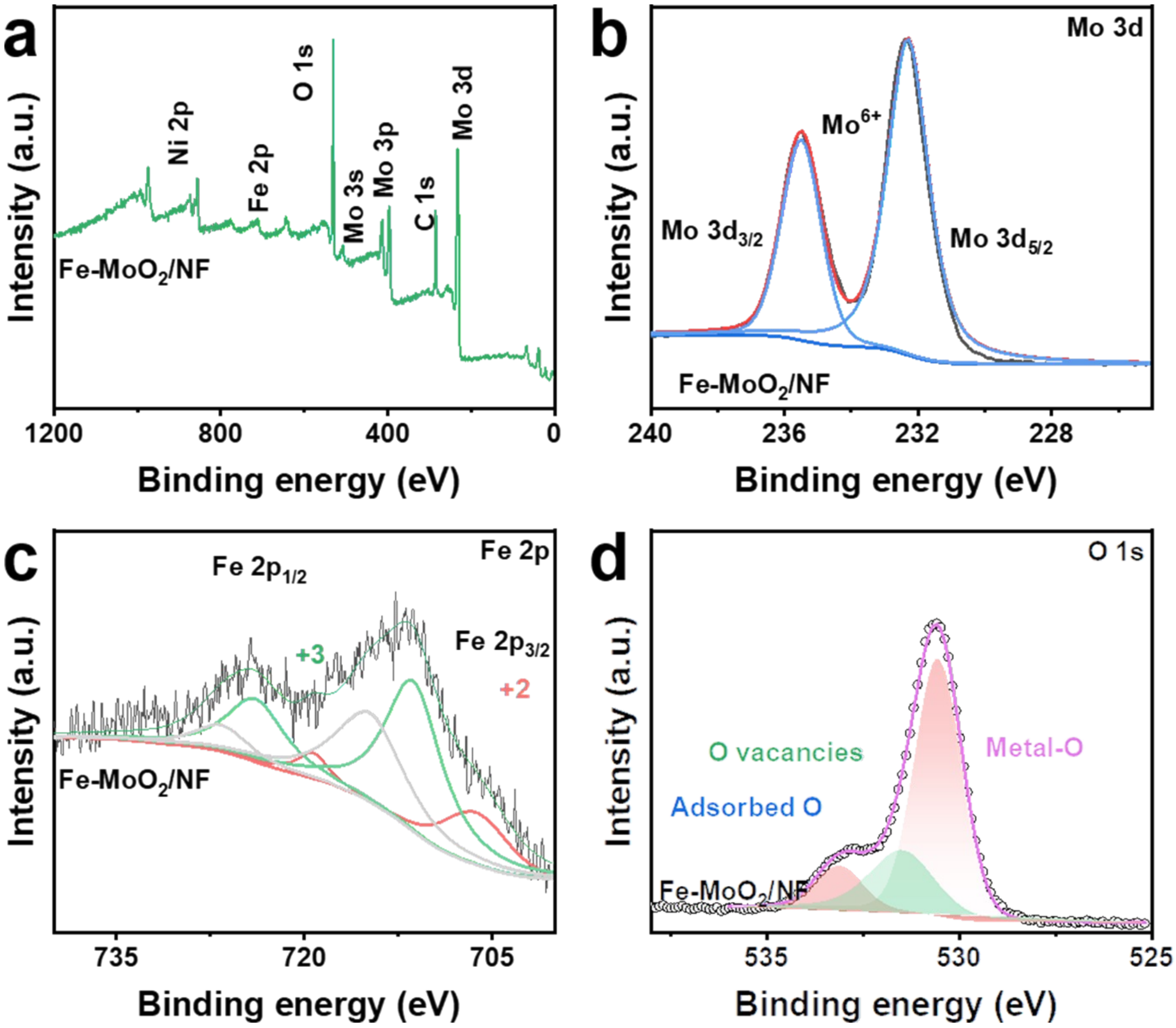

Figure S28. (a) XPS survey spectrum and high-resolution spectra of: (b) Mo 3d, (c) Fe 2p, and (d) O 1s for Fe- MoO$_2$/NF after OER process.

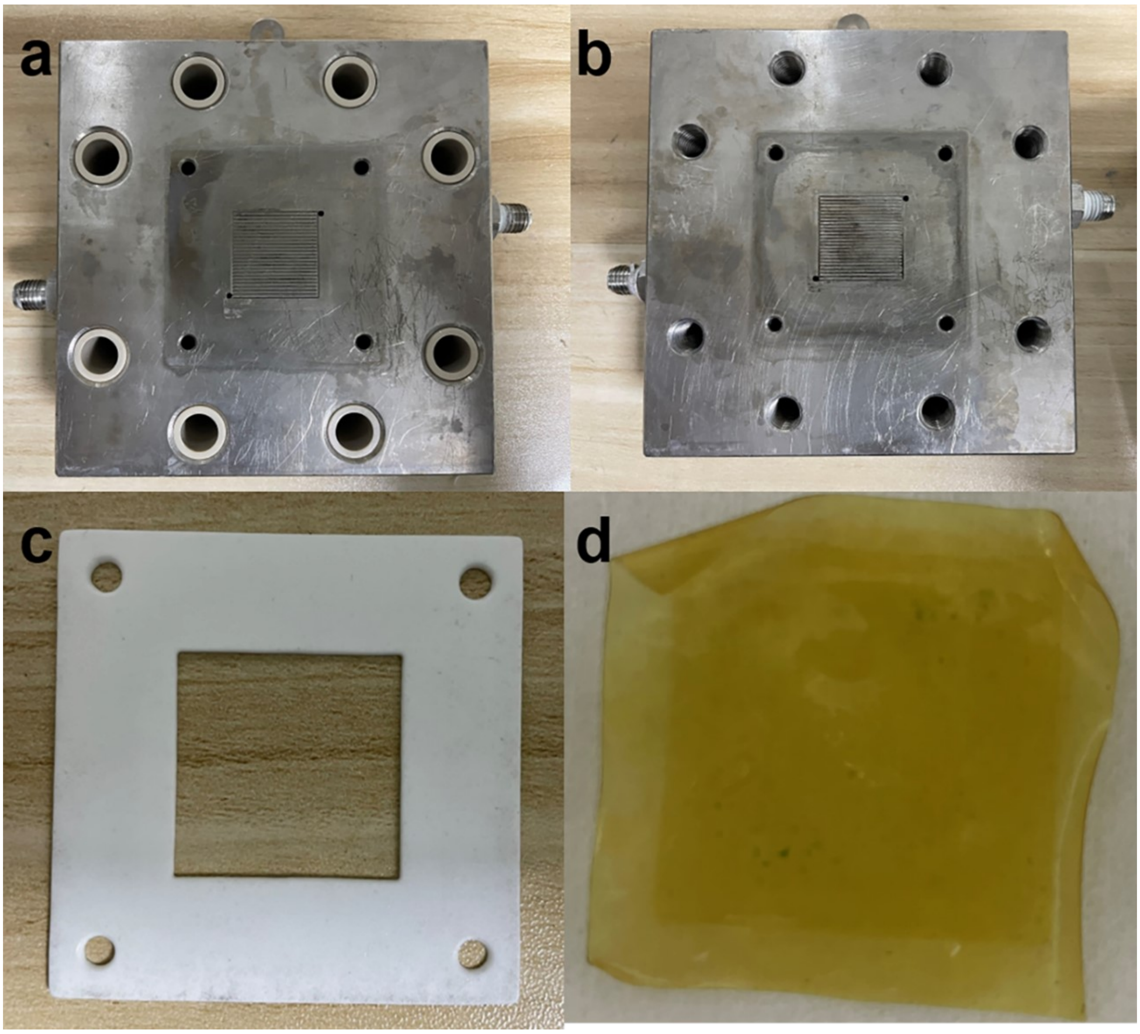

Figure S29. Home-made AEM electrolyzer.

S3 Table

Table S1 The atomic contents of Mo, Fe and O at the surface of FeMoO/NF, MoO_2/NF, Fe-MoO_x/NF, as-prepared Fe-MoO_2/NF, post-HER Fe-MoO_2/NF, and post-OER Fe-MoO_2/NF.

	Mo （Atomic %）	**Fe （Atomic %）**	**O （Atomic %）**
Fe-MoO_2/NF	25.8%	4.3%	69.9%
MoO_2/NF	30.4%	--	69.6%
FeMoO/NF	18.2%	2.0%	79.8%
Fe-MoO_x/NF	21.5%	8.4%	70.1%
Fe-MoO_2/NF (post-HER)	24.9%	5.0%	70.1%
Fe-MoO_2/NF (post-OER)	17.9%	7.2%	74.9%

Table S2 The positions of Mo, Fe and O species at the surface of FeMoO/NF, MoO$_2$/NF, Fe-MoO$_x$/NF, as-prepared Fe-MoO$_2$/NF, post-HER Fe-MoO$_2$/NF, and post-OER Fe-MoO$_2$/NF.

	Mo（eV）		**O（eV）**			**Fe（eV）**	
	Mo^{6+}	**Mo^{4+}**	**Metal-O**	**O vacancies**	**Adsorbed O**	**Fe^{3+}**	**Fe^{2+}**
Fe-MoO$_2$/NF	235.3, 230.4	232.5, 229.3	530.3	531.5	532.7	723.7, 710.8	719.2, 706.2
MoO$_2$/NF	235.4, 230.8	232.8, 229.6	531.1	532.4	533.6	--	--
FeMoO/NF	235.2, 232.1	--	530.4	--	532.3	723.9, 711.3	719.3, 706.3
Fe-MoO$_x$/NF	235.4, 230.1	232.4, 229.1	530.6	531.8	532.5	723.4, 710.8	719.1, 706.2
Fe-MoO$_2$/NF (post-HER)	235.2, 230.4	232.4, 229.2	530.3	531.8	532.9	723.8, 710.1	719.2, 706.7
Fe-MoO$_2$/NF (post-OER)	235.8, 232.3	--	530.5	531.4	533.1	724.1 711.4	719.3, 706.4

Table S3 The percentages of Mo, Fe and O species at the surface of FeMoO/NF, MoO_2/NF, Fe-MoO_x/NF, as-prepared Fe-MoO_2/NF, post-HER Fe-MoO_2/NF, and post-OER Fe-MoO_2/NF.

	Mo（eV）		**O（eV）**			**Fe（eV）**	
	Mo^{4+}	**Mo^{6+}**	**Metal-O**	**O vacancies**	**Adsorbed O**	**Fe^{3+}**	**Fe^{2+}**
Fe-MoO_2/NF	70.3%	29.7%	62.5%	25.3%	12.2%	66.7%	33.3%
MoO_2/NF	64.7%	35.3%	70.6%	17.7%	11.7%	--	--
FeMoO/NF	--	100%	69.3%	--	30.7%	72.3%	27.7%
Fe-MoO_x/NF	58.0%	42.0%	67.4%	14.5%	18.1%	71.6%	28.4%
Fe-MoO_2/NF (post-HER)	70.1%	29.9%	77.3%	12.2%	10.5%	69.3%	30.7%
Fe-MoO_2/NF (post-OER)	--	100%	65.8%	23.7%	10.5%	77.0%	23.0%

Table S4. Structure parameters extracted from the EXAFS fitting of Mo K-edge of Fe–MoO_2/NF, MoO_2 and Mo foil, respectively.

	shell	**CN**	**R(Å)**	**σ^2**	**ΔE_0**	**R factor**
Mo foil	Mo-Mo	8	2.72±0.01	0.0038	4.0±0.9	0.0017
	Mo-Mo	6	3.13±0.01	0.0033		
MoO_2	Mo-O1	2	1.63±0.01	0.0056		
	Mo-O2	4	2.03±0.01	0.0014		
	Mo-Mo	1	2.58±0.01	0.0032		
Fe–MoO_2/NF	Mo-O	4.8±0.2	2.00±0.01	0.0027	-0.3±1.2	0.0072
	Mo-Mo	0.9±0.1	2.53±0.01	0.0024		

[a] *CN*: coordination numbers; [b] *R*: bond distance; [c] σ^2: Debye-Waller factors; [d] ΔE_0: the inner potential correction. *R* factor: goodness of fit. S_0^2 was set to 0.70, according to the experimental EXAFS fit of Mo foil reference by fixing CN as the known crystallographic value; δ: percentage.

As shown in Table S4, the coordination numbers (CN) and bond distances (R) obtained for Fe-MoO_2/NF were obviously different from MoO_2/NF. Among them, the total Mo coordination number in Fe-MoO_2/NF is 5.7 in comparison with 7 in MoO_2. The total Mo-O bond distance in Fe–MoO_2/NF is 2.00 Å compared to 2.03 Å in MoO_2. The results suggest that Fe-MoO_2/NF had a lower CN of Mo and a shorter interatomic distance of the Mo-O bond.

Table S5 Calculated free energies of adsorption of intermediates for MoO_2 and Fe-MoO_2 at U = 0 V.

	OH*（eV）	**O*（eV）**	**OOH*（eV）**	**O_2（eV）**
Fe-MoO_2	-0.74	0.56	2.59	4.92
MoO_2	-1.6	-0.4	1.5	4.92

Table S6 HER performance of prepared catalysts in alkaline seawater (units: mV).

	Pt/C/NF	**Fe-MoO$_2$/NF**	**MoO$_2$/NF**	**MoO$_3$/NF**	**FeMoO/NF**
η10	38	17	33	311	294
η100	173	119	157	487	438
η200	262	178	220	493	--
	NF	**Fe-MoO$_X$/NF**	**Co-MoO$_2$/NF**	**Ni-MoO$_2$/NF**	
η10	253	104	22	15	
η100	369	168	91	81	
η200	432	--	--	--	

Table S7 HER performance of prepared catalysts in alkaline water (units: mV).

	Pt/C/NF	**Fe-MoO$_2$/NF**	**MoO$_2$/NF**	**MoO$_3$/NF**	**FeMoO/NF**	**NF**
η10	19	16	32	294	282	253
η100	138	89	155	428	419	426
η200	226	132	208	517	489	428

Table S8 Rct value of prepared catalysts in alkaline seawater at -17 mV *vs.* RHE.

	Fe-MoO_2/NF	**MoO_2/NF**	**FeMoO/NF**	**MoO_3/NF**	**NF**
Rct (Ω)	2.2	7.4	300	320	112

Table S9 HER performance of recently reported catalysts.

Catalysts	Electrolyte	η_{10} (mV)	η_{100} (mV)	Tafel (mV dec^{-1})	Reference
Fe-MoO_2/NF	1 M KOH	16	89	58	**This work**
Fe-MoO_2/NF	1 M KOH Seawater	17	119	71	**This work**
MoO_2/Mo_3P/Mo_2C	1 M KOH	69		60.4	*Small 2023, 19, 2206472.*
MoO_2/Co	1 M KOH	48	117	49.5	*J. Mater. Chem. A, 2022, 10, 17297–17306.*
NiMoFe NPs@MoO_2 NPAs	1 M KOH		79	33	*J. Mater. Chem. A, 2022, 10, 3760–3770.*
Ni_3P/MoP_2/MoO_2	1 M KOH	3		65.7	*J. Mater. Chem. A, 2021, 9, 25934–25943.*
Ni-MoO_2/NF-IH	1 M KOH	39		75	*Adv. Funct. Mater. 2021, 31, 2009580.*
MoO_2/MoS_2/C	1 M KOH	91	270	49	*Adv. Funct. Mater. 2021, 31, 2101715.*
MoO_3-MoO_2@NiMo	1M NaOH	33.4		96.8	*J. Mater. Chem. A, 2021, 9, 3677–3684.*
h-NiMoFe	1 M KOH	14		32.7	*Energy Environ. Sci., 2021, 14, 4610–4619.*
Ni@C-MoO_2/NF	1 M KOH	25		44.23	*J. Mater. Chem. A, 2020, 8, 14545–14554.*
CoP/MoO_2	1 M KOH	29	87	50	*J. Mater. Chem. A, 2020, 8, 16018–16023*
CoP-MoO_2/MF	1 M KOH	42		127	*J. Mater. Chem. A, 2020, 8, 6732–6739.*
MoO_2-FeP@C	1 M KOH	103		48	*Adv. Mater. 2020, 32, 2000455.*
NiMoO-SP/Ti	1 M KOH	159		77	*Nanoscale, 2017, 9, 17349–17356.*
Porous MoO_2	1 M KOH	27		54	*Adv. Mater. 2016, 28, 3785–3790.*
Ru/MoO_{2-x}	1 M KOH	29		22	*Appl. Catal. B, 2022, 307, 121204-121212.*
Ni/MoO_{2-x}	1 M KOH	27	95	26	*Chem. Eng. J. 2023, 464, 142671-142681.*
(Ni,Fe)OOH/MoO_2	1 M KOH seawater	20	140	23.2	*Appl. Catal. B, 2024, 340, 123277-123294*
$(NiFeCoV)S_2$	1 M KOH seawater	110	255	58.23	*J. Colloid Interface Sci, 2023, 645, 724-734*
Ni_2P-Fe_2P/NF	1 M KOH seawater	129	251	86	*Adv. Funct. Mater.2021, 31, 2006484*
Cu-CoFe/Co/NC	1 M KOH seawater	217		114.9	*Chem. Eng. J. 2023, 451, 138699-138707*

Table S10 Comparison of synthesis methods of Mo-based catalysts.

Catalysts	Synthetic method	T (°C)	Time (h)	Ref.
Fe-MoO_2	**Carbothermal shocking**	**820**	**127s**	**This work**
$Ni_xMo_{1-x}O_2$	Tube furnace heating	450	1-2h	*ACS Energy Lett. 2020, 5,1908-1915.*
MoO_2	Tube furnace heating	650	2h	*Chem. Eng. J. 2022, 427, 131309-131318*
MoO_2/C	Tube furnace heating	650	2h	*ACS Energy Lett. 2020, 5, 3237-3243*
MoO_2/MoS_2|P	Tube furnace heating	700	40min	*Appl. Catal. B: Environ. 2020, 266, 118649-118657*
$MoNi_4$/MoO_2@Ni	Tube furnace heating	500	2h	*Nat Commun, 2017, 8, 15437*
MoO_2/MoS_2/C	Tube furnace heating	900	3h	*Adv. Funct. Mater. 2021, 31, 2101715-2101724*
MoO_2-FeP	Tube furnace heating	400	1h	*Adv. Mater. 2020, 32, 2000455-2000464.*
MoO_2-Ni	Tube furnace heating	550	2h	*ACS Catalysis, 2019, 9, 2275-2285*
Co-N-doped MoO_2	Tube furnace heating	450;650	1-2h	*Nano Energy, 2017, 41, 772-779.*
Ru/MoO_2	Tube furnace heating	350	2h	*Appl. Catal. B, 2022, 307, 121204-121211.*
MoO_2/MoS_2	Tube furnace heating	400	1h	*Appl Surf Sci, 2020, 504, 144291-144296*
CoP/MoO_x-CC	Tube furnace heating	300	2h	*J. Mater. Chem. A, 2020, 8,16018-16023.*

Table S11 Comparison of carbothermal shocking and Tube furnace heating methods.

	Carbothermal shocking	**Tube furnace heating**
Heating rate	~13°C/s	~10°C/min
Cooling rate	~32°C/s	~5°C/min
Reaction time	127 s	2 h
Mo oxidation state	low	high
HER overpotential	17 mV@10 mA cm^{-2}	100 mV@10 mA cm^{-2}

Table S12 OER performance of prepared catalysts in alkaline seawater (Units: mV).

	RuO_2/NF	**Fe-MoO_2/NF**	**MoO_2/NF**	**MoO_3/NF**	**FeMoO/NF**	**NF**
η50	500	310	440	480	340	710
η100	640	340	500	540	390	--
η200	750	380	570	610	430	--

Table S13 OER performance of prepared catalysts in alkaline water (Units: mV).

	Fe-MoO$_2$/NF	**MoO$_2$/NF**	**MoO$_3$/NF**	**FeMoO/NF**
η50	280	410	440	310
η100	300	470	500	340
η200	330	540	570	390

Table S14 OER performance of recently reported catalysts.

Catalysts	Electrolyte	η_{10} (mV)	η_{100} (mV)	Tafel (mV dec^{-1})	Reference
Fe-MoO$_2$/NF	**1 M KOH**	**--**	**300**	**64**	**This work**
Fe-MoO$_2$/NF	**1 M KOH Seawater**	**--**	**340**	**75**	**This work**
NiMoFe NPs@MoO$_2$ NPAs	1 M KOH	--	246	35	*J. Mater. Chem. A, 2022, 10, 3760–3770.*
Ni@C–MoO$_2$/NF	1 M KOH	240	--	52.34	*J. Mater. Chem. A, 2020, 8, 14545–14554.*
MoO$_2$–Co$_2$Mo$_3$O$_8$@C	1 M KOH	320	--	88	*Chem. Commun., 2018, 54, 2739-2742.*
NiMoO-SP/Ti	1 M KOH	280	360	85	*Nanoscale, 2017, 9, 17349–17356.*
Porous MoO$_2$	1 M KOH	260	--	54	*Adv. Mater. 2016, 28, 3785–3790.*
RuMoNi	1 M KOH seawater	245	291	41.2	*Nat. Commun, 2023, 14, 3607-3617.*
(NiFeCoV)S$_2$	1 M KOH seawater	--	299	49.51	*J. Colloid Interface Sci. 2023, 645, 724–734.*
Ni$_2$P-Fe$_2$P/NF	1 M KOH seawater	240	305	58	*Adv. Funct. Mater.2021, 31, 2006484.*
NiMoO$_4$@NiFeP	1 M KOH seawater	--	282	50.7	*ACS Sustainable Chem. Eng. 2023, 11, 22, 8362–8373.*
NiTe@FeOOH	1 M KOH seawater	--	280	52	*Chem. Eng. J. 2023, 474, 145568-145575*

Table S15 The current and energy consumption table.

	100 mA (kW·h/m^3)	**150 mA (kW·h/m^3)**	**250 mA (kW·h/m^3)**	**350 mA (kW·h/m^3)**
Ni foam 25℃	6.6	7.8	8.6	9.9
Fe-MoO$_2$/NF 25℃	5.5	6.4	7.7	8.5
Fe-MoO$_2$/NF 50℃	4.2	5.2	6.2	6.8